A study on coupling effect between sloshing and motion of FLNG with partially filled tanks

Tsuyoshi Kawahashi[1], Makoto Arai[1], Xin Wang[2], Liang-Yee Cheng[3], Kazuo Nishimoto[3], Akira Nakashima[1]

DOI: 10.1007/s00773-018-0596-5
The final publication is available at link.springer.com.
https://link.springer.com/article/10.1007%2Fs00773-018-0596-5

Abstract This paper discusses the coupling influence of floating LNG (FLNG) motions with internal liquid sloshing. Model experiments were performed in an ocean model basin, and results were compared with numerical calculations. The FLNG model used in our study had 6 square tanks. In order to verify the liquid cargo effect, the FLNG model was tested under two conditions: a liquid-cargo condition and a fixed solid-cargo condition. As for filling level, there were three loading conditions (15%, 50%, and 90% filled). Our numerical scheme solves internal liquid sloshing using a three-dimensional finite difference method, and ship motion by potential theory. The sloshing effect was computed by the time-domain coupled simulation. We obtained good agreement between experimental and numerical results even at the near-natural frequency of sloshing. In both experimental results and numerical simulations, the effect of internal liquid is significant for sway and roll motion. Furthermore, the internal free surface motions obtained by the experiments and numerical simulations showed similar non-linear free surface behavior in the case of low filling.

Tsuyoshi Kawahashi
Email: kawahashi-tsuyoshi-fd@ynu.jp

[1] Department of Systems Design for Ocean-Space, Yokohama National University, 79-5 Tokiwadai, Hodogaya-ku, Yokohama, Japan

[2] Faculty of Science, Agriculture and Engineering, Newcastle University, NE1 7RU, UK

[3] University of Sao Paulo, Av. Prof. Mello Moraes, 2231, Cidade Universitária CEP05508-900, SP, Brazil

Keywords FLNG, ship motion, nonlinear sloshing, coupling effect, liquefied natural gas

1 Introduction

The demand for natural gas is rapidly growing. Natural gas has attracted attention because it is one of the cleanest fossil fuels, with high energy efficiency, lower CO_2 emission, and no emission of SO_x. For better storage and transportation efficiency, natural gas is usually cooled and converted to a liquid form (LNG). It has been estimated that about 60% of all natural gas worldwide is contained in ocean reservoirs. New natural gas fields are being discovered in more remote and deeper ocean areas. It is not feasible to use pipelines for these gas fields due to long distances, and it is likely that floating LNG (FLNG) will be used for the exploitation of these fields. The FLNG is a new type of floating platform for producing, liquefying, storing, and offloading natural gas at offshore locations. Although there has been some researches on the technological challenges of FLNG in recent years, much work is still needed to achieve fully satisfactory solutions for some of the problems. One of them is the sloshing of LNG and its effects on FLNG motion.

In contrast to LNG carriers, it is inevitable that filling conditions will be varied in a FLNG during production and offloading process. In addition, large tanks are necessary to store LNG, and the membrane system is preferred for space efficiency. In membrane tanks, violent sloshing is likely to occur around the tanks' natural period, and this may affect the motion of FLNG significantly. The large motion of FLNG may increase production downtime. During offloading operations, large motions also increase the risk of collision with the shuttle tanker. Similar problems may also occur with floating storage and regasification unit (FSRU) and its shuttle tankers, and with LNG fuel ships and its bunkering ships.

To investigate and elucidate the coupled sloshing and ship-motion problem, several model tests have been conducted. Molin et al. [1] performed a model test of a rectangular barge with two partially filled tanks on the deck in regular and irregular beam waves. The model test was mainly aimed at validating the numerical method developed within the software Diodore (principia). The experimental results showed that the nonlinearities of sloshing dynamics, especially at the low filling level, are important for accurate prediction of ship motion.

As part of the SALT joint industry project, MARIN conducted model tests on coupled sloshing and motion responses for an LNG carrier and a box-type FLNG [2]. The effects of sloshing on first- and second-order motion at three filling levels have been investigated. ExxonMobil has also conducted a model test of a large LNG carrier [3]. Both these experiments demonstrated that coupling effects significantly influence lateral motion, with a much smaller effect on longitudinal motion. Nasar et al. [4] investigated coupled sloshing and ship motion using a barge with one rectangular tank in regular beam waves. Nonlinear sloshing behavior in regular wave excitations was observed and further investigated. Nam et al. [5] conducted a series of model tests for a LNG FPSO with two prismatic tanks. Regular waves were generated during the experiment. The aim of the experiment was to validate the developed numerical method. It was demonstrated that the nonlinearities of sloshing-induced forces and moments have significant effects on ship motion.

Besides the model tests, many numerical methods have also been developed to study the coupling effects between sloshing and ship motion. These methods can be categorized into two approaches: the frequency-domain approach and time-domain approach. The frequency-domain approach is based on the linear potential flow model for both internal and external flow fields. Hydrodynamic coefficients due to sloshing, radiation and diffraction coefficients, and wave forces are calculated separately by solving the linear internal and external flow fields, respectively. To obtain reasonable results around the sloshing resonant frequency, damping is usually included in the internal sloshing calculation. Representative studies using the frequency-domain approach can be found in Molin et al. [1], Malenica et al. [6,7], and Zalar et al. [8]. For the time-domain approach, a reasonable choice is to use a hybrid approach, where the linear potential flow model is applied to the radiation/diffraction problems, and a direct Navier-Stokes solver is applied to the sloshing problem. Kim et al. [9,10] developed such a hybrid method. They obtained the radiation/diffraction coefficients and wave forces in the frequency domain based on linear theory. The simulation of ship motion was carried out using the convolutional integral method. The particle method and finite difference method were used for sloshing simulations. Lee at al. [11] and Lee and Kim [12] developed a similar method, using convolution integrals of linear hydrodynamic coefficients for ship-motion prediction, and a finite difference method to solve the internal sloshing problem. Bunnik and Veldman [13] also developed a method with a linear potential theory for the radiation/diffraction problem and a VOF method for the sloshing problem. In addition to the hybrid approach, various other numerical methods have been developed. Hashimoto et al. [14] solved the ship motion problem based on a nonlinear potential flow model. The sloshing dynamics were accounted for using the particle method. Faltinsen and Timokha [15,16] presented analytically-based nonlinear multimodal methods for the sloshing problem. This method was coupled with a linear potential theory for the external flow to study the coupling effects between sloshing and ship motion [17]. Mitra et al. [18,19] developed a coupled algorithm using a hybrid marine control system for ship-motion simulation and a finite element method for nonlinear sloshing. Nakashima et al. [20] and Manderbacka et al. [21] applied pendulum models to obtain sloshing forces with low computational load. These simplified models, although application may be restricted to some specific limits, can give benchmark data to CFD computations.

Results of the experimental and numerical studies described above indicate that:

1. Sloshing dynamics have significant effects on lateral ship motion while the effects on longitudinal motion are more limited
2. The resonant frequency of roll motion will be shifted due to the sloshing coupling effect, and a secondary roll peak appears near the natural frequency of transverse sloshing
3. For the global behavior of coupled sloshing and ship motion, the nonlinearities of the external flow are less important except for viscous roll damping, and the nonlinearities of the sloshing dynamics are critical in accurately predicting the coupling effects.

Wang and Arai [22-24] developed a hybrid time-domain numerical method for the coupled sloshing and ship-motion problem. The external flow field was solved by the linear potential theory and the internal sloshing flow was solved by a three-dimensional (3-D) finite difference method. The method was validated by comparison with existing model test results [25]. Applications of this method may be found in [26,27]. In the present paper, the numerical method developed by Wang and Arai is further validated by comparison with a model test of a FLNG carried out at the University of Sao Paulo [28]. Based on the numerical and experimental results, we investigated the coupling effects on ship motion and internal free surface movement. We focus discussion on the nonlinearities at the low filling level and its effects on ship motion and present new findings on the coupling effect at the low filling level.

2 Numerical method

2.1 Sloshing problem

Internal liquid sloshing was computed by the 3-D finite difference method-based scheme developed by Arai and Cheng [29-31]. A staggered mesh system was applied to solve the fluid field using a grid cell, as shown in Fig. 1. The flow is assumed to be laminar.

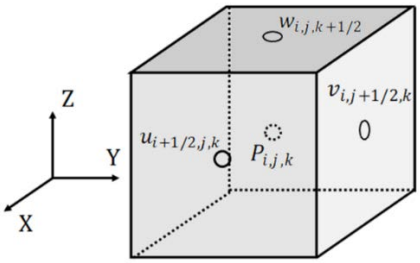

Fig. 1 Arrangement of finite different variables and coordinate system

Navier-Stokes equations expressed in the finite difference form are:

$$u_{i+\frac{1}{2},j,k}^{n+1} = u_{i+\frac{1}{2},j,k}^{n} + \delta t \left\{ \frac{1}{\rho \delta x}\left(p_{i,j,k}^{n} - p_{i+1,j,k}^{n}\right) + \frac{f_x^n}{\rho} - \left[\frac{\partial u^2}{\partial x}\right]_{i+\frac{1}{2},j,k}^{n} - \left[\frac{\partial uv}{\partial y}\right]_{i+\frac{1}{2},j,k}^{n} - \left[\frac{\partial uw}{\partial z}\right]_{i+\frac{1}{2},j,k}^{n} + \nu[\nabla^2 u]_{i+\frac{1}{2},j,k}^{n} \right\} \quad (1\text{-}1)$$

$$v_{i,j+\frac{1}{2},k}^{n+1} = v_{i,j+\frac{1}{2},k}^{n} + \delta t \left\{ \frac{1}{\rho \delta y}\left(p_{i,j,k}^{n} - p_{i,j+1,k}^{n}\right) + \frac{f_y^n}{\rho} - \left[\frac{\partial vu}{\partial x}\right]_{i,j+\frac{1}{2},k}^{n} - \left[\frac{\partial v^2}{\partial y}\right]_{i,j+\frac{1}{2},k}^{n} - \left[\frac{\partial vw}{\partial z}\right]_{i,j+\frac{1}{2},k}^{n} + \nu[\nabla^2 v]_{i,j+\frac{1}{2},k}^{n} \right\} \quad (1\text{-}2)$$

$$w_{i,j,k+\frac{1}{2}}^{n+1} = w_{i,j,k+\frac{1}{2}}^{n} + \delta t \left\{ \frac{1}{\rho \delta z}\left(p_{i,j,k}^{n} - p_{i,j,k+1}^{n}\right) + \frac{f_z^n}{\rho} - \left[\frac{\partial wu}{\partial x}\right]_{i,j,k+\frac{1}{2}}^{n} - \left[\frac{\partial wv}{\partial y}\right]_{i,j,k+\frac{1}{2}}^{n} - \left[\frac{\partial w^2}{\partial z}\right]_{i,j,k+\frac{1}{2}}^{n} + \nu[\nabla^2 w]_{i,j,k+\frac{1}{2}}^{n} \right\} \quad (1\text{-}3)$$

where

u, v, w: velocity components with respect to the coordinates fixed to the tank

p: pressure

$f_x,\ f_y, f_z$: external forces in the x, y and z directions

δt: period for a time step

$\delta_x,\ \delta_y, \delta_z$: cell dimensions in x, y and z directions

ρ: liquid density

ν: kinematic viscosity of liquid

The velocity components were calculated at each time step by Eq. 1. The continuity equation (Eq. 2) was used to correct the velocity components by adjusting the pressure field using an iteration algorithm (Hirt et al. [32]).

$$\frac{\partial u}{\partial x} + \frac{\partial v}{\partial y} + \frac{\partial w}{\partial z} = 0 \quad (2)$$

In order to calculate the position of the free surface, a single-valued height function *h* was utilized. The free surface height (*h*) was renewed at every time step by evaluating the kinematic condition:

$$\frac{\partial h}{\partial t} + u\frac{\partial h}{\partial x} + v\frac{\partial h}{\partial y} = w \quad (3)$$

With this method, local free-surface deformations such as wave-breaking cannot be simulated, but the method is stable to obtain global sloshing phenomena even in the resonant state.

To solve the coupled problem, estimation of the force and moment from liquid motion is also important. They were obtained by

$$F = \int_s\ p\vec{n}_i dS \quad (4)$$

$$M = \int_S\ p(\vec{r}_G \times \vec{n}_i) dS \quad (5)$$

integrating the pressure along the tank walls.

where

$\vec{n}_i$: normal vector of the tank wall

$\vec{r}_G$: vector point to center of gravity

2.2 Ship-motion problem

The ship-motion problem was solved using a well-known strip theory, the Salvesen-Tuck-Faltinsen method (STF method) [33]. A 2-D boundary element method was used to solve the diffraction and radiation problem at each section. The sloshing simulation explained above was coupled with the ship motion simulation in the time-domain to consider the coupling effect. The following equation (Eq. 6) was used to obtain the ship motion.

$$\boldsymbol{M}\ddot{\boldsymbol{X}}(t) + \boldsymbol{C}\dot{\boldsymbol{X}}(t) + \boldsymbol{K}\boldsymbol{X}(t) = \boldsymbol{F_D}(t) + \boldsymbol{F_{slosh}}(t) \quad (6)$$

where

$\boldsymbol{M}$: the generalized mass matrix;

$\boldsymbol{X}$: the vector of ship motion displacements;

$\boldsymbol{C}$: damping matrix due to radiation calculated by the STF method;

$\boldsymbol{K}$: linear hydrostatic restoring matrix;

$\boldsymbol{F_D}$: diffraction force/moment vector calculated by the STF method;

$\boldsymbol{F_{slosh}}$: slosh-induced force/moment vector.

In Eq. 6, the surge motion of the ship was neglected. Therefore, the dimensions of $\boldsymbol{M}$, $\boldsymbol{C}$, and $\boldsymbol{K}$ are (5×5), and the dimensions of $\boldsymbol{X}$, $\dot{\boldsymbol{X}}$, $\ddot{\boldsymbol{X}}$, $\boldsymbol{F_D}$, and $\boldsymbol{F_{slosh}}$ are (5×1).

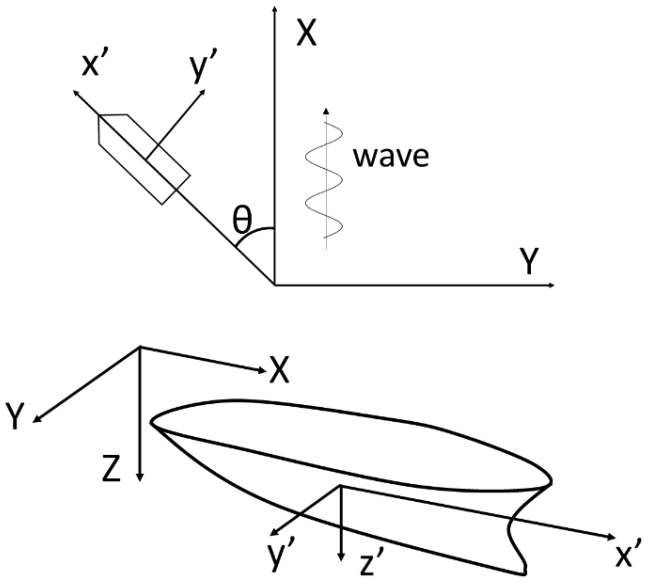

Fig. 2 Coordinate systems of ship-motion calculations

Fig. 2 shows the coordinate systems used in this calculation. The XYZ-coordinate system is earth fixed, and the x'y'z'-coordinate system is body-fixed. θ represents the relative angle between ship speed and wave direction; θ=180° represents the head-wave condition; and θ=90° denotes the beam-wave condition.

In the present research, we focused on the coupling effect and response in regular waves, and thus the memory effect is not considered when solving the motion equation in time domain. In Eq. 6, the linear added mass and damping coefficients are calculated by the STF method for the same frequency as the incident wave. Similarly, the linear diffraction force is calculated as $\boldsymbol{F_D}(t) = \Re\{\boldsymbol{E}(\omega)e^{i\omega t}\}$, where $\boldsymbol{E}(\omega)$ is the vector of complex wave diffraction force amplitude.

For the linear ship motion responses in regular waves, the present approach will give exactly the same results as the convolution formulation approach (memory effect). However, as the sloshing forces are now considered in the ship motion equation, the nonlinear sloshing response will add force components with different frequencies into the system. Thus, the convolution formulation may provide some improvement in accuracy. Based on the comparison between numerical and experimental results presented in this paper, we believe that the accuracy of the present approach without memory effect is satisfactory for regular wave conditions. One of our future works will be to apply the convolution formulation for irregular wave conditions and also investigate its influence in regular waves. To solve Eq. 6 in a time domain, Newmark's β method was employed

$$\ddot{\boldsymbol{X}}(t+dt) = \left\{\boldsymbol{M} + \left(\frac{dt}{2}\right)\boldsymbol{C} + \beta(dt)^2\boldsymbol{K}\right\}^{-1} \cdot \left[\boldsymbol{F}(t+dt) - \boldsymbol{C}\left\{\dot{\boldsymbol{X}}(t) + \frac{dt}{2}\ddot{\boldsymbol{X}}(t)\right\} - \boldsymbol{K}\left\{\boldsymbol{X}(t) + dt\dot{\boldsymbol{X}}(t) + \left(\frac{1}{2}-\beta\right)(dt)^2\ddot{\boldsymbol{X}}(t)\right\}\right] \quad (7\text{-}1)$$

$$\dot{\boldsymbol{X}}(\mathrm{t}+\Delta\mathrm{t}) = \dot{\boldsymbol{X}}(\mathrm{t}) + \left(\frac{dt}{2}\right)\left\{\ddot{\boldsymbol{X}}(t) + \ddot{\boldsymbol{X}}(t+dt)\right\} \quad (7\text{-}2)$$

$$\mathbf{X}(\mathrm{t}+\mathrm{dt}) = \mathbf{X}(\mathrm{t}) + \frac{dt}{1!}\dot{\boldsymbol{X}}(t) + \frac{(dt)^2}{2!}\ddot{\boldsymbol{X}}(t) + \beta(dt)^3\frac{\ddot{\boldsymbol{X}}(t+dt) - \ddot{\boldsymbol{X}}(t)}{dt} \quad (7\text{-}3)$$

(Eq. 7). β was set at 0.25 for reasons of numerical stability.

Here, $\boldsymbol{F}(t) = \boldsymbol{F_D}(t) + \boldsymbol{F_{slosh}}(t)$.

The authors have also tested another version of the numerical code which uses fourth order Runge-Kutta method, and for this particular application, no significant difference was found between the two methods.

In the strip method, the restoring forces for sway and yaw are zero; therefore, the numerical simulation may cause a divergence problem. In order to solve the problem and obtain stable numerical results, artificial springs are added for sway and yaw motions. The stiffness of the horizontal artificial spring for each section is assumed to be

$$\mathrm{k} = c_k \cdot \left(\frac{\omega_e}{2}\right)^2 \cdot m_x \quad (8\text{-}1)$$

where

c_k: coefficient that controls the strength of the artificial spring

ω_e: encounter frequency

m_x: sectional mass of the ship

Following the strip method scheme, the total restoring forces in sway and yaw motions can be derived. Thus, the sway and yaw components of the linear hydrostatic restoring matrix $\boldsymbol{K}$ are given as

$$K_{22} = c_k \cdot \left(\frac{\omega_e}{2}\right)^2 \cdot m_{22} \quad (8\text{-}2)$$

$$K_{66} = c_k \cdot \left(\frac{\omega_e}{2}\right)^2 \cdot m_{66} \quad (8\text{-}3)$$

where K_{22} and K_{66} are the sway and yaw restoring coefficients respectively, and m_{22} and m_{66} are the mass (or moment of inertia) of the sway and yaw motions.

The artificial spring is applied for ocean-going ships who do not have a mooring system, e.g., LNG carriers. The value of c_k should be chosen as small as possible, so that its effect on the transverse motion responses is negligible. This can be done by comparing the frequency domain linear RAO results with and without the artificial spring. For offshore applications like FLNG, the linear stiffness of the mooring system from the actual project or model test can be used directly as the value of K_{22} and K_{66}.

Fig. 3 shows the flow chart of the computation for solving the coupled ship motions and sloshing problem. The details of this method and its experimental validation can be found in references [22-24].

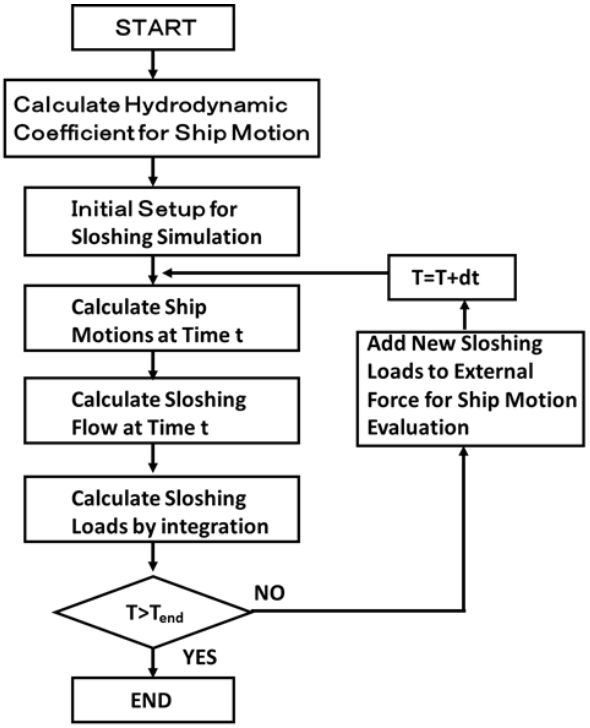

Fig. 3 Flow chart of numerical simulation

3 FLNG Model particulars

In order to validate our numerical method, we compared the numerical results with Rocha et al.'s model experiment on a 1:110 scaled FLNG model with 6 rectangular tanks [28]. The FLNG model here was tested under 6 conditions, with fixed solid ballast and with liquid cargo in its tanks, and at 3 filling levels (15%, 50% and 90%). Fresh water was used as liquid cargo and filled the 6 tanks equally.

The layout and dimensions of the model used in the experiment are shown in Fig. 4 and Table 1. The grid numbers of the tanks are 29x30x30 in longitudinal, transverse and vertical directions of the tanks.

In this study, the value of c_k for the artificial spring is chosen as 0.1. By comparing the frequency domain linear RAO results with and without this artificial spring, it has been confirmed that the effect of the artificial spring is insignificant. This value of c_k does not reflect the true stiffness of the springs used in the model test. This may have a certain effect on the results of the sway and yaw motions, and it is

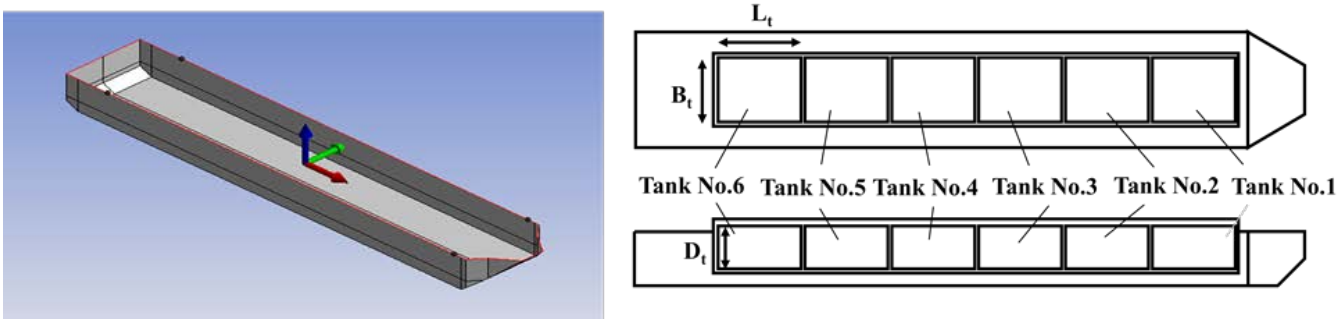

Fig. 4 The layout of the tanks in the FLNG model

Table 1 The principal particulars of ship and tanks

Particulars		Value			Unit
		15%Load	50%Load	90%Load	
L_{pp}	Length between perpendiculars		450		m
Breadth			81		m
Depth			38		m
Draft		12.2	16.6	22.0	m
Submarged Volume		432364	591683	788592	ton
KG	Vertical center of gravity	22.99	18.53	20.85	m
LCG	Longitudinal center of gravity	-13.7	-13.16	-12.45	m
GM_t	Transverse metacentric height	28.76	23.27	15.38	m
GM_t'	Transverse metacentric height (free-surface effect adjusted)	22.56	18.74	11.98	m
I_{xx}	Roll moment of inertia	4.39×10^8	4.00×10^8	4.63×10^8	m^4
I_{yy}	Pitch moment of inertia	6.17×10^9	8.62×10^9	1.12×10^{10}	m^4
I_{ZZ}	Yaw moment of inertia	6.12×10^9	8.71×10^9	1.13×10^{10}	m^4
T_{roll}	Natural roll periods of the ship	15.43	13.82	16.11	sec
L_t	Tank length		58.41		m
B_t	Tank breadth		45.10		m
D_t	Tank depth		29.04		m
T_n	Natural sloshing periods	13.98	8.67	7.79	sec

discussed in the following section.

4 Numerical results and discussion

In this article, we focused on the linear RAOs for the ship motion responses. We compared the response amplitude operators (RAOs) obtained by the numerical method with the experimental results (see Figs. 5 and 12). Fig. 5 shows the beam wave (90-degree wave) condition, and Fig. 12 the 135-degree wave condition. In addition, in order to study the internal liquid effect on ship motion, the results obtained by our numerical method were compared with the ship motion response with fixed solid cargo. The numerical results with fixed solid cargo were calculated by a potential theory. The FLNG does not have advanced speed. Regular waves, 2.0[m] high in actual scale, were used in both the experiment and numerical calculations.

Fig. 5 presents the RAOs of ship motions in beam waves. The numerical results agreed well with the experimental ones for both the liquid cargo conditions and solid cargo. The internal liquid effect on the FLNG motion can be clearly observed by comparing the test results of liquid and solid cargo cases. For heave motion, there was not a clear difference between the two cargo conditions. The liquid cargo motion does not affect the heave motion in the beam waves. On the other hand, for sway and roll motion in the beam waves, the liquid cargo had a significant effect on the ship motion. In particular, the effects under the low filling (15% filling) condition were different from the high filling (50% and 90% filling) conditions. For sway motion, a large peak appeared in the RAO for each filling level. As for roll motion, when the liquid cargo was loaded, the natural period of the ship-roll motion increased. This trend could also be seen generally at each filling level. Under 15% filling, the sway and roll motion RAO fluctuated irregularly at a period of around 15.0[s], and another large peak appeared in roll motion RAO at 11.5[s].

It is worth mentioning that some discrepancy can be found in the sway RAO at around the roll natural period, especially for 15% and 50% filling conditions. During the experiment, springs were used to control the sway and yaw motions and simulate some mooring effects. As explained in the previous section, the artificial spring employed in the numerical calculation did not reflect the true values of the springs used in the model experiment. The authors believe that this is the primary reason for discrepancy observed in the sway RAO in Fig. 5. However, in general, there were good agreements between the experimental and calculated results.

In order to examine the liquid cargo effect, we investigated the liquid cargo's force in the sway direction, and liquid cargo's rolling moment (Figs. 6a, 6b). The point of reference for moment around x-axis is the COG of the ship without cargo. The phase difference

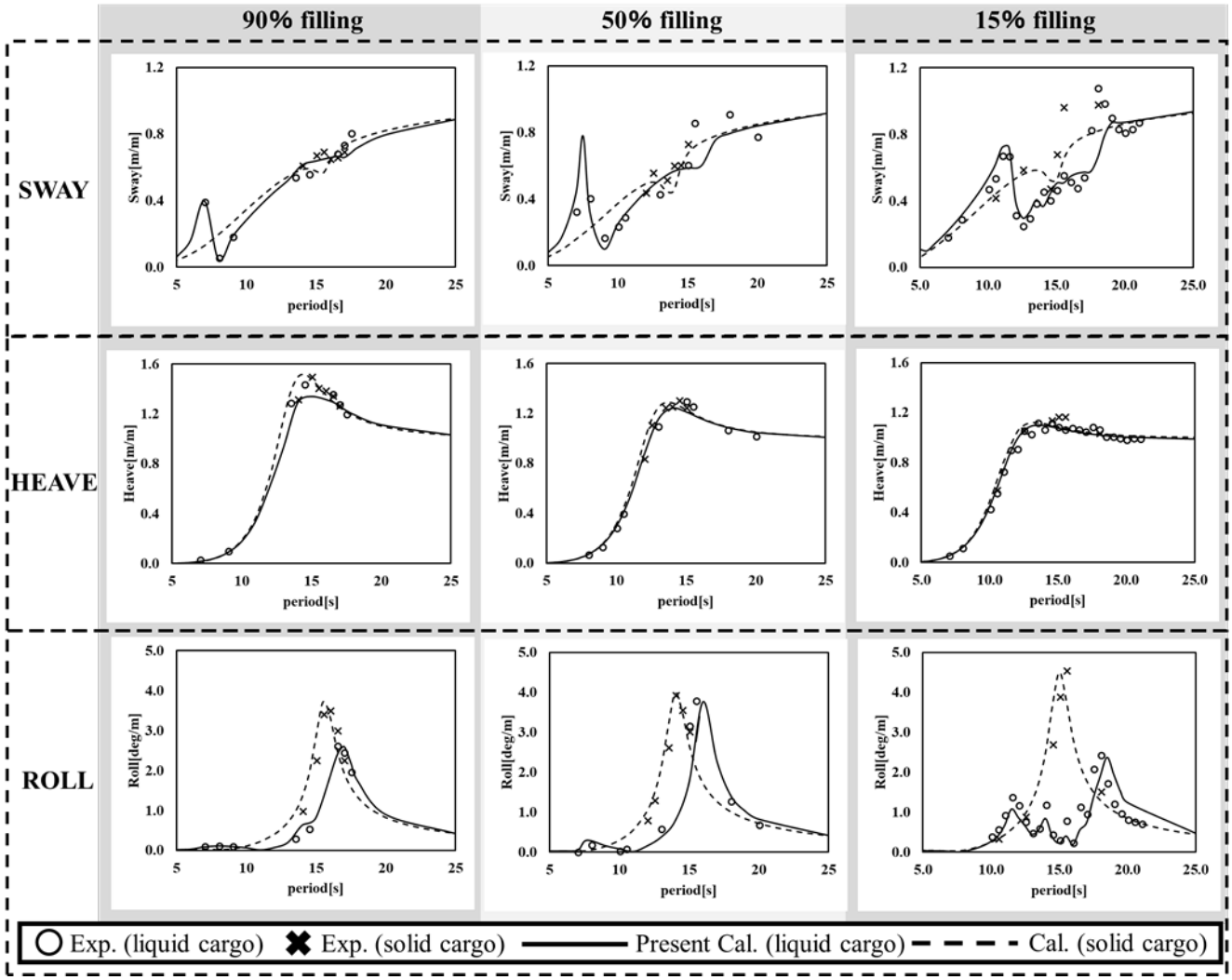

Fig. 5 Amplitude of motions for 90-degree waves

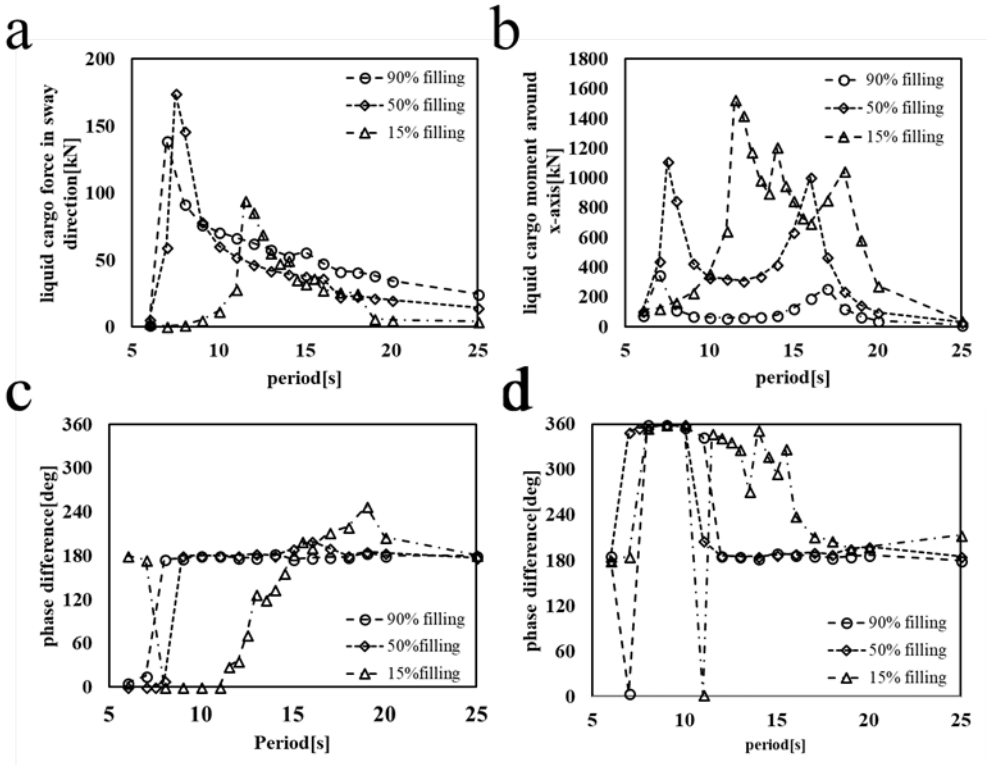

Fig. 6 (a) Liquid cargo force in sway direction in beam wave. (b) Rolling moment from liquid cargo for beam wave. (c) Phase difference between the force and FLNG acceleration. (d) Phase difference between the rolling moment caused by the liquid cargo and the roll angular acceleration .

between the force in sway direction and ship sway motion acceleration (Fig. 6c), and the phase difference between the rolling moment caused by liquid cargo and the roll motion acceleration (Fig. 6d) were also investigated. The natural periods of the liquid cargo motion in the tank in the sway direction were 7.8[s] (90% filling), 8.7[s] (50% filling), and 14.0[s] (15% filling). The natural periods were estimated by a linear theory. (Eq. 9)

$$T_n = 2\pi \Big/ \sqrt{g \frac{\pi}{B_t} \tanh h \frac{\pi}{B_t}} \tag{9}$$

For the 50% and 90% filling conditions, the sway force peak and rolling moment peak appeared at around the tank's natural periods as estimated by the linear theory. However, for the 15% filling condition, the peak period was different from the natural period when estimated in this manner. In Fig. 6c,when the ship motion period is smaller than the peak period of sway motion, the phase difference between liquid cargo force and ship motion acceleration was 0 degrees for each filling level. In this situation the internal liquid amplifies the motion of FLNG. We could therefore conclude that the large peak in sway RAO for each filling level was caused by resonances between ship motion and sloshing inside the tanks. The phase difference changed to 180 degrees suddenly at the sloshing natural period for the 50% and 90% filling conditions. When the phase difference was 180 degrees, the internal liquid reduced the ship motion. The sway RAO curve coupled with liquid cargo was lower than those with fixed solid cargo at periods longer than the peak period. Meanwhile, for the 15% filling condition, the phase-difference behavior diverged from the high filling conditions.

The phase changed gradually in a wide range of periods, and had a more significant influence on the sway and roll motions. This phase changing caused the RAO fluctuations.

For roll motion, Fig. 6b shows the rolling moment of the liquid cargo, and Fig. 6d presents the phase difference between that rolling moment and the FLNG roll-motion acceleration. The moment of the liquid cargo (Fig. 6b) had two peaks in the 50% and 90% filling conditions. The first was at the sloshing resonant period and the second at the ship motion natural period. In the 15% filling condition, the rolling moment of the liquid cargo had three peaks. The first peak was due to sloshing resonance, the second was at the period when hydraulic bore occured, and the third peak was at the ship roll-motion natural period. For each filling, at around the first peak period of the liquid cargo's moment, the phase difference between the cargo's rolling moment and roll acceleration was around 0 degrees. The liquid motion was resonant with the ship roll motion. Actually, the roll motions coupled with liquid cargo in Fig. 5 show slightly higher values than those of the FLNG with fixed solid cargo cases at around the first peak period of the liquid cargo's moment.With increasing periods, the phase difference changed to 180-degrees for the 50% and 90% filling conditions, with the liquid cargo tanks acting as anti-rolling tanks. The same situation occured in the 15% filling conditions, i.e., at the natural period of ship roll motion, in which the phase is about 180-degrees, the cargo tanks acted as anti-rolling tanks.

For the roll motion, the shift of the ship motion natural period occurred for each filling level. This roll natural period shift was mainly caused by the static free-surface effect. When a vessel with a partially filled tank is heeled, the free surface of the liquid remains parallel to the horizontal line. The center of gravity of the liquid, which is the center of its volume, will move with the liquid and can have a considerable effect upon vessel stability. The free-surface effect can be estimated by Eq.10, where $\overline{GM}$ is the transverse metacentric height, $\overline{GM'}$ is the transverse metacentric height considering the free-surface effect, V is the displacement, and i_j is the moment of inertia of the area around the center of floatation.

$$\overline{GM'} = \overline{GM} - \sum_k \frac{i_j}{V} \tag{10}$$

This decreased stability caused by the free-surface effect induced the natural period of the roll motion to shift towards longer periods. By using $\overline{GM'}$, the shift of roll natural frequency can be easily predicted without simulating the sloshing flow in the tank. In Fig.7, the solid line and dotted line were calculated by potential theory without calculating free surface motion. The natural period has shifted to a longer period. From Fig. 7, it is evident that the shift of the roll natural period is mainly caused by the decreased stability.

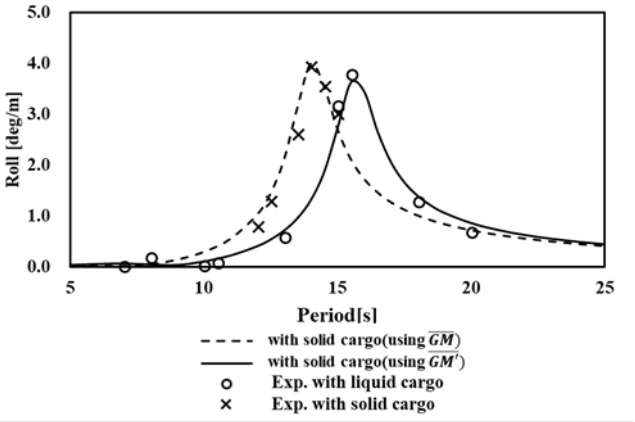

Fig. 7 Free-surface effect

We also investigated sloshing flow in the tanks. Fig. 8 compares the measured and computed free-surface motion in the No. 6 tank at around the tank's natural period. The excitation period for 90% filling was 7.0[s], 50% filling 8.0[s], and 15% filling 14.0[s]. Measured and computed free surface motion were in good agreement even at the periods when the largest free surface movement occurred. We also compared the measured and computed free-surface motion at other periods and confirmed that there was good agreement between measured and computed values.

Several different free surface modes were found by investigating the free surface motion. These different modes caused different liquid cargo force and moment. Therefore, the influence on the ship motion was also varied. In addition, there were differences in free surface motion between the low filling condition (15%) and high filling conditions (50% and 90%). With the high filling conditions, the liquid cargo motion inside the tank could be divided into two types. When the ship motion period was near the natural period of sloshing, significant sloshing was generated. The free-surface elevation rose when the period was close to the tank natural period. When sloshing

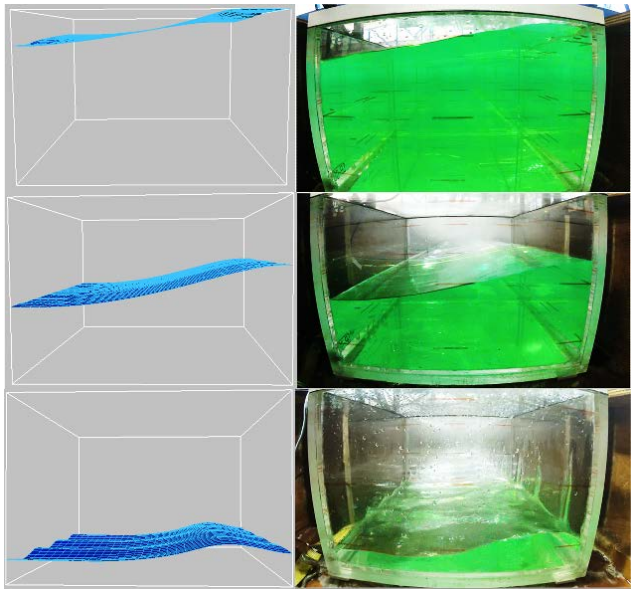

Fig. 8 Free surface deformations in resonant period for different filling conditions (Top: 90%, Middle : 50%, Bottom: 15%)

occurred, the liquid cargo force became highest for the 50% and 90% filling levels. In Fig. 6a, the highest value of the force in the sway direction occurred at 50% filling. This was because the free-surface elevation was higher than at 90% filling, as shown in Fig. 8. In the 90% filling condition, liquid mass was heavier than in the 50% filling condition. However since the liquid motion was restricted by the tank ceiling, the force was smaller than that of 50% filling. When the ship motion period was longer than the natural period of the tank, a "planar wave" appeared. The liquid cargo's force and moment for the planar wave were relatively small.

Fig. 9 compares the free-surface deformation, the time histories of the liquid cargo's force in the sway direction, and its rolling moment for the sloshing and planar wave modes (i.e., 7.0[s]. and 15.0[s]). At T=15.0[s], since the excitation period is far longer than the resonant period, free surface deformation is very small, and it remains almost flat. In this mode, the free surface movement in the tank appears to follow the roll motion in the tank-fixed coordinates. If the earth-fixed coordinates are used, the free surface almost remains as a horizontal plane. We call it "planar wave" in this paper. For sloshing and planar

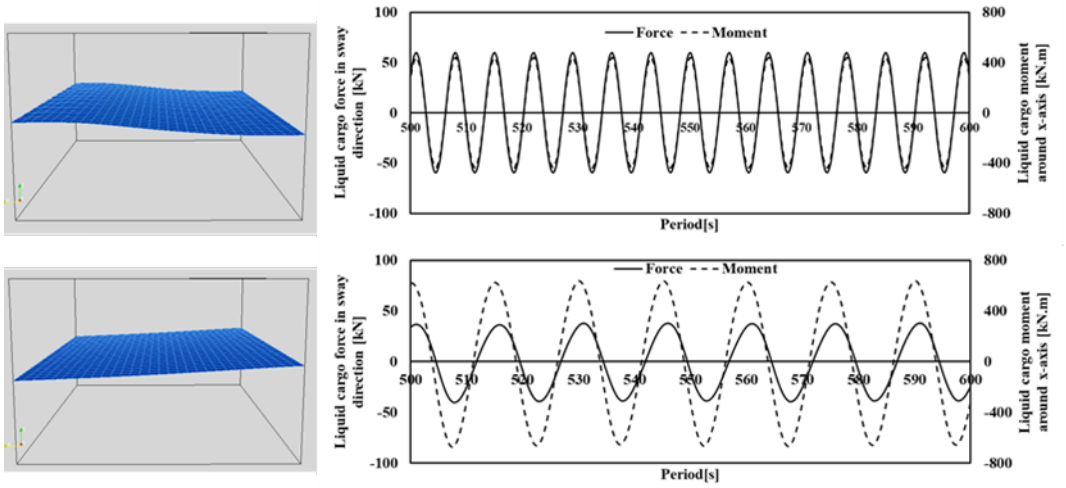

Fig. 9 Free surface deformation and time histories of force in sway direction and rolling-moment for 50% filling (Top : sloshing T=7.0[s], Bottom : planar wave T=15.0[s])

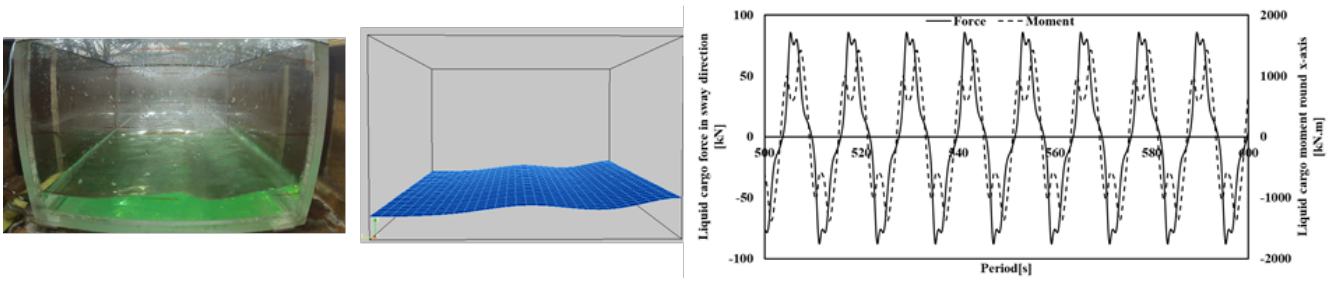

Fig. 10 Free surface deformation and time histories of force in sway direction and rolling-moment of the hydraulic bore for 15% filling (T=12.0[s])

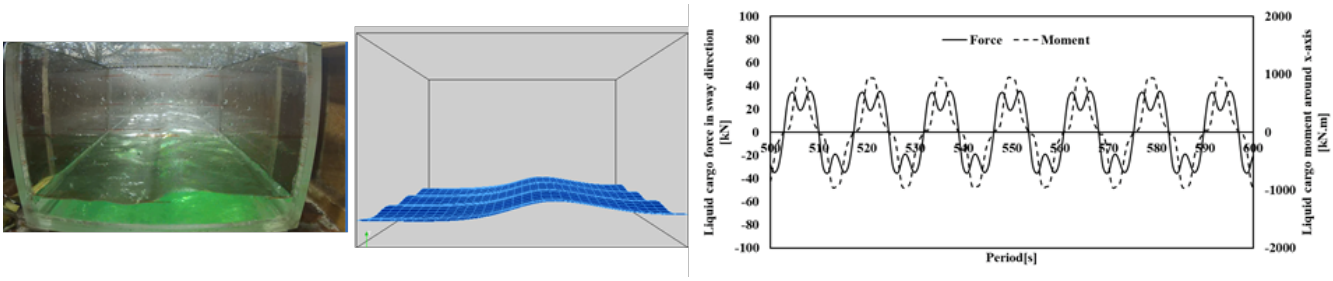

Fig. 11 Free surface deformation and time histories of force in sway direction and rolling-moment of the small traveling waves for 15% filling (T=14.5[s])

waves, the time histories of the cargo's force and moment were simple steady, and the cycle of both force and moment were in the same phase as the ship motion period.

For the low filling condition, there were 4 different types of free surface motion. At a short period (5.0-11.0[s]), sloshing was observed. This was similar to the high filling conditions. At periods longer than the sloshing state, but still smaller than the tank's natural period (11.5-13.5[s]), a hydraulic bore appeared (Fig. 10). At periods longer than the natural period of the tank (14.0-18.5[s]), short travelling waves occurred (Fig. 11). At much longer periods (19.0[s] or more), a planar wave appeared. Fig. 10 shows the free-surface deformation and time histories of the liquid cargo's force and moment when

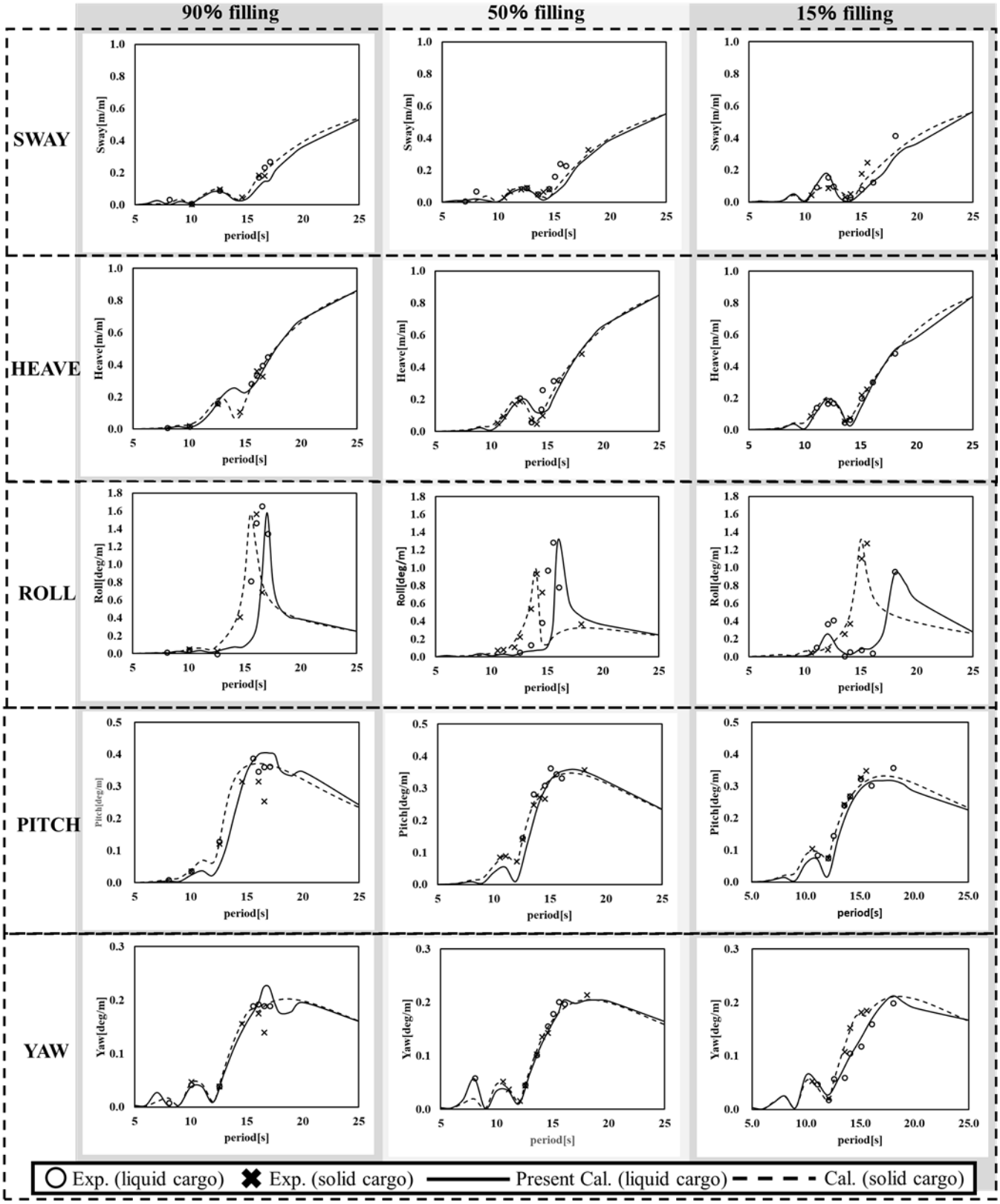

Fig. 12 Amplitude of motions for 135-degree waves

hydraulic bore occurred. Hydraulic bore often causes high liquid-cargo force, which in turn leads to larger rolling moment on the ship. In Fig. 6b, at the period when the hydraulic bore occurred, the liquid cargo's rolling moment was higher than those of the high filling conditions. In the 15% filling condition, the amount of liquid cargo movement became violent. Fig. 11 shows the free-surface deformation and time histories of force and moment for the short traveling waves. The cycle of the planar wave is the same as that of the ship motion period. The small traveling waves also generated rather large force and moment because of the large motion of the liquid.

Fig. 12 presents the RAOs for 135-degree waves. The numerical results were in good agreement with the experimental ones for both the liquid cargo and solid cargo conditions. Similar to Fig. 5, agreement was less good in the sway RAO at around the roll natural period. As explained above, the reason is that the artificial spring employed in the numerical calculation did not reflect the true values of the springs used in the model experiment.

Comparing the liquid cargo and fixed solid cargo cases for 135-degree waves, we found no significant differences, except for the roll response. For the 50% and 90% filling cases, the roll natural period shifted to a longer period as in the beam wave condition. In the 15% filling case, due to the lack of the experimental data, the natural period of the roll motion is not clear. The liquid-cargo force and moment are shown in Figs. 13 and 14, respectively. In these figures, the values of the liquid cargo's force and moment for the 135-degree wave were about 1/10 values of the beam wave condition. As for the liquid cargo force, the 90% filling condition showed the highest value and the15% filling condition the lowest value in general. This is because the force
mainly depends on the mass of the liquid cargo. However, in the low filling condition (i.e., 15% filling) a high peak of the force is observed where an intensive liquid motion occurs. For the liquid cargo rolling moment, the 15% filling condition showed the highest value. In the low filling condition, the amount of the liquid cargo motion was the largest.

Sloshing flow in the tanks for 50% and 90% filling conditions showed, free surface motion similar to the beam wave cases, but free surface amplitudes were very small. In contrast, for the 15% filling condition, the free surface motion was a little different from that of the beam wave condition. At a short period (around T=12.0[s]), sloshing appeared. For periods longer than the sloshing state, at T=13.0[s] and 14.0[s], hydraulic bore was generated. At T=15.0[s] and 16.0[s], small traveling waves were observed. At T=17.0[s], hydraulic bore appeared in the longitudinal direction (Fig. 15). At T=18.0-20.0[s], small traveling waves appeared in the longitudinal direction. For this low filling condition, the liquid-cargo motion's natural period in the longitudinal direction was estimated to be 17.9[s], where the free surface motion was at resonance in the longitudinal direction.

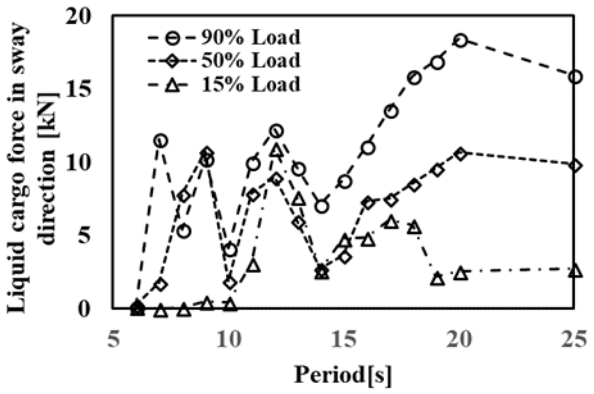

Fig. 13 Liquid cargo force in sway direction for 135-degree wave

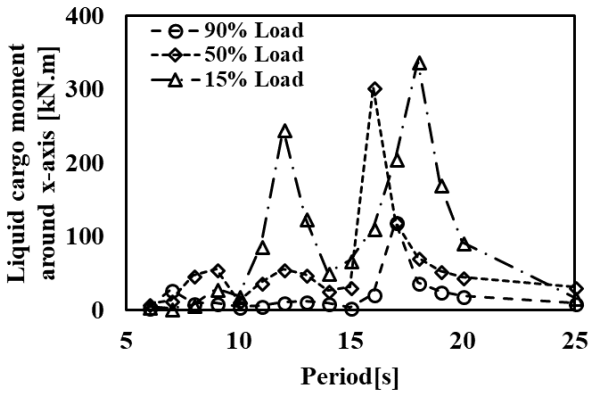

Fig. 14 Liquid cargo moment around x-axis for 135-degree wave

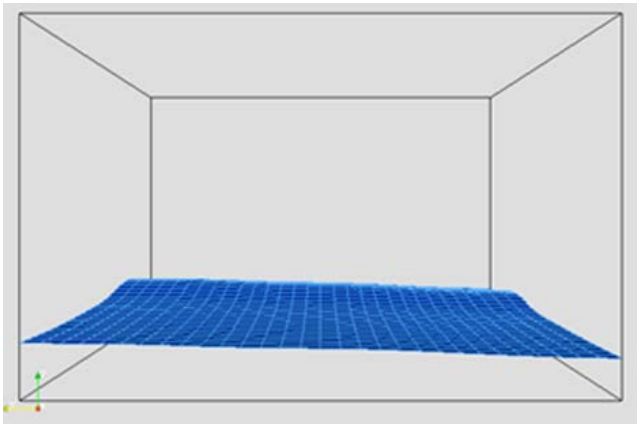

Fig.15 Free surface motion at T=17.0[s] in 135-degree wave

5 Conclusions

Based on the results of the numerical and experimental studies we conducted on the coupled effect between sloshing and FLNG motion, we drew the following conclusions:

- The present numerical method can reproduce the coupled FLNG motion with highly non-linear free surface behavior in liquid cargo tanks.
- The free surface inside the tanks does not significantly influence heave, pitch or yaw motions. On the other hand, the liquid inside the tank affects the ship motion in transverse motion markedly, i.e., in sway and roll. In sway motion, at around the natural periods of the internal liquid motion, the response becomes noticeably higher. The response was

largest at 50% filling. In roll motion, the natural period increase is caused by the decreased stability due to the free-surface effect. In the low filling condition, peaks due to the ship motion natural period and tank sloshing natural period were observed.

- In the low filling condition, the response of the FLNG motion becomes irregular in sway and roll due to the non-linear sloshing effect. The free surface motion can be divided into 4 types: sloshing, planar wave, hydraulic bore and small traveling waves. These different waves have different impacts on ship motion.
- In the 135-degree wave condition, the effects of the liquid cargo are not significant. The shift of the natural periods of the roll motion is caused by the decreased stability, which appears regardless of the wave direction.
- In the 135-degree wave condition, the free surface motion is small. However, longitudinal liquid motion occurs at around the free suface motion's natural period in the longitudinal direction.

Our future works:

- As shown in the paper, we observed the generation of the waves in the tank's longitudinal direction at the sloshing natural period in the longitudinal direction of the tank. Its effect on the ship motion is our next research theme.
- The presented method can be applied to the estimation of the damping effect of ant-rolling tanks, which may also be our future research work.

References

1. Molin B, Remy F, Rigaud S, De Jouette C (2002) LNG FPSO's: frequency domain, coupled analysis of support and liquid cargo Motion. Proceedings of the 10th International Maritime Association of the Mediterranean (IMAM) Conference, Rethymnon, Greece
2. Gaillarde G, Ledoux A, Lynch M (2004) Coupling between liquefied gas and vessel's motion for partially filled tanks: Effect on seakeeping. Design and operation of gas carriers
3. Huang Z J, Esenkov O E, O'Donnell B J, Yung T W, Martin C B, Danaczko M A, &others (2009) Coupled tank sloshing and LNG carrier motions. The Nineteenth International Offshore and Polar Engineering Conference
4. Nasar T, Sannasiraj S A, Sundar V (2008) Experimental study of liquid sloshing dynamics in a barge carrying tank. Fluid Dynamics Research 40: 427-458
5. Nam B-W, Kim Y, Kim D-W, Kim Y-S (2009) Experimental and numerical studies on ship motion responses coupled with sloshing in waves. Journal of Ship Research 53: 68-82
6. Malenica S, Zalar M, Chen X B (2003) Dynamic coupling of seakeeping and sloshing. Proceedings of the 13th international offshore and polar engineering conference 3: 486-492
7. Malenica Zalar M, Orozco J M, Le Gallo B, Chen X B (2004) Linear and nonlinear effects of sloshing on ship motions. 23rd OMAE, Conference, Vancouver, Canada
8. Zalar M, Diebold L, Baudin E, Henry J, Chen X-B (2007) Sloshing effects accounting for dynamic coupling between vessel and tank liquid motion. 26th OMAE Conference, San Diego, USA.
9. Kim Y (2007) Experimental and numerical analyses of sloshing flows. Journal of Engineering Mathematics, 58: 191-210
10. Kim Y, Nam B W, Kim D W, Kim Y S (2007) Study on coupling effects of ship motion and sloshing. Ocean Engineering, 34: 2176-2187
11. Lee S J, Kim M H, Lee D H, Shin Y S (2007) The Effects of tank sloshing on LNG vessel responses. Proceedings of the 26 the International Conference on Offshore Mechanics and Arctic Engineering
12. Lee S J, Kim M H (2010) The effects of inner-liquid motion on LNG vessel responses. Journal of Offshore Mechanics and Arctic Engineering, 132: 021101
13. Bunnik T, Veldman A (2010) Modelling the effect of sloshing on ship motions. Proceedings of the 29th International Conference on Offshore Mechanics and Artic Engineering (OMAE2010), Shanghai, China, June: 6-11
14. Hashimoto H, Ito Y, Sugimoto T, Sueyoshi M (2010) Numerical simulation of dynamic coupled motions of ship and tank liquid. Proceedings of the 5th Asia-Pacific Workshop on Marine Hydrodynamics, Osaka, Japan
15. Faltinsen O M, Timokha A N (2009) Sloshing with ship applications. Proceedings of the 13th International Conference of Association of the Mediterranean, Istanbul, Turkey
16. Faltinsen O M, Timokha A N (2014) Sloshing. Cambridge University Press
17. Rognebakke O F, Faltinsen O M (2003) Coupling of sloshing and ship motions. Journal of Ship Research, 47: 208-221
18. Mitra S, Hai L V, Jing L, Khoo B C (2012) A fully coupled ship motion and sloshing analysis in various container geometries. Journal of marine science and technology, 17: 139-153
19. Mitra S, Wang C Z, Reddy J N, Khoo B C (2012) A 3D fully coupled analysis of nonlinear sloshing and ship motion. Ocean Engineering, 39: 1-13
20. Nakashima A, Arai M, Nishimoto K (2017) Influence of Liquid Sloshing on FLNG Motion, Journal of the Japan Society of Naval Architects and Ocean Engineers, 26: 81-91
21. Manderbacka T L, Jacob V, Carriot T, Mikkola T, Matusiak J E (2014) Sloshing forces on a tank with two compartments, application of the pendulum model and CFD, Proceedings of the International Conference on Offshore Mechanics and Arctic Engineering (OMAE)
22. Wang X, Arai M (2011) Research on computational method of coupled ship motions and sloshing. Journal of the Japan Society of Naval Architects and Ocean Engineers, 14: 97-104
23. Wang X, Arai M (2011) A study on coupling effect between seakeeping and sloshing for membrane-type LNG carrier. International Journal of Offshore and Polar

Engineering, 21(04)
24. Wang X, Arai M (2015) A numerical study on coupled sloshing and ship motions of a liquefied natural gas carrier in regular and irregular waves. Proceedings of the Institution of Mechanical Engineers, Part M: Journal of engineering for the maritime environment, 229(1): 3-13
25. Yamashita S (1981) Motions of a Floating Body with a Liquid Storage Tank. Journal of West-Japan society Naval Architecture, 61: 155-165
26. Arai M, Suzuki R, Ohta Y, Wang X (2012) Study of an anti-sloshing floating device for membrane-type LNG tanks, Proceedings of IMDC 2012, 11th International Marine Design Conference, 2: 554-565
27. Arai M, Cheng L Y, Wang X, Okamoto N, Hata R, Karuka G (2016) Sloshing and swirling behavior of liquid in a spherical LNG tank. Proceedings of PRADS2016
28. Rocha T P, Dotta R, Vieira D P, Mello P C D, Malta E B, Nishimoto K (2015, October) Experimental Investigation on the Influence of Liquid Cargo in Floating Vessels Motions. OTC Brasil. Offshore Technology Conference
29. Arai M, Cheng L Y, Kumano A, Miyamoto T (2002) Technique for Stable Numerical Assessment of Hydrodynamic Impact Pressure in Sloshing Simulation. Journal of the Society of Naval Architects, Japan, 191: 299-309
30. Cheng L Y, Arai M (2003) A Technique for Stable Numerical Assessment of Hydrodynamic Impact Pressure Due to Sloshing in Chamfered Tanks. Conference Proceedings, The Society of Naval Architects of Japan, 1: 105-106
31. Cheng L Y, & Arai M (2005) A 3D Numerical Method for Assessment of Impact Loads Due to Sloshing in Liquid Cargo Tanks. Proceedings of the Fifteenth International Offshore and Polar Engineering Conference, Seoul, Korea: 214-221
32. Hirt CW, Nichols BD, Romero NC (1975) SOLA—A Numerical Solution Algorithm for Transient Fluid Flows. Los Alamos Scient Lab Report, LA-5852
33. Salvensen N, Tuck E O, Faltinsen O (1970) Ship motions and sea loads, Transactions, Society of Naval Architects and Marine Engineers, 78: 250-287